Orientation effects in the Coulomb-explosion ionization of an H_2^+ wave packet by short xuv pulses: Applicability of the fixed-nuclei approximation

Morten Førre[1,2] and Henri Bachau[1]

[1]*Centre Lasers Intenses et Applications, Université Bordeaux 1-CNRS-CEA, 351 Cours de la Libération, F-33405 Talence Cedex, France*

[2]*Department of Physics and Technology, University of Bergen, N-5007 Bergen, Norway*

The Coulomb explosion ionization process of an H_2^+ wave packet in xuv laser fields has been studied by fully three-dimensional *ab initio* wave packet calculations, with moving nuclei, beyond the Born-Oppenheimer approximation. Both the cases of parallel and perpendicular orientation of the molecule with respect to the laser field have been investigated. Furthermore, we have examined the applicability of the fixed-nuclei approximation method to obtain the kinetic energy distribution of the released nuclei. It is found that the approximation breaks down already at relatively short pulses. We also show that the relative orientation of the internuclear axis and polarization vector has a crucial effect on the kinetic energy spectrum.

I. INTRODUCTION

Intense femtosecond (fs) infrared (ir) laser pulses are currently used to produce time-resolved spectra at the atomic or molecular time scales [1,2] while tremendous progresses have been realized in the domain of ultrashort xuv fields [3,4]. In parallel with source developments, detection techniques have also considerably improved. Pump-probe setups combined with sophisticated spectrometers now provide high-resolution multidimensional real-time mapping of H_2^+ and D_2^+ nuclear wave packets at the sub-fs time scale [5]. The possibility of using femtosecond lasers acting on a manifold of molecular vibrational states to encode quantum information has been previously studied [6]. Pump-probe techniques are explored in view of controlling selective transfer of populations in molecules [7]. In this context, techniques such as laser Coulomb explosion imaging (LCEI) with ultrashort xuv fields could be used to characterize nondestructively the coherent vibrational wave packet at the femtosecond time scale. Thus, pump-probe-type techniques applied to the fastest vibrational motion in nature—the hydrogen stretch within a molecule—have a large potential of applications: from imaging to coherent control and quantum information processing. Therefore, it is necessary to develop theoretical methods to describe the dynamics of simple molecular systems interacting with strong and short laser fields.

In contrast to the case of one- and two-electron atoms, full-dimensional quantum calculations for the interaction of molecules with intense light, treating all the electronic and nuclear degrees of freedom on an equal footing, have not yet been performed, even for the simplest molecular systems H_2^+ and D_2^+. This is mainly due to the increased complexity introduced by the nuclear motion, and the fact that the electronic and nuclear dynamics usually occurs on completely different time scales, with the additional difficulty, in the ir domain, that a large number of photons are involved. Therefore, in most applications to molecules, the time-dependent Schrödinger equation (TDSE) is solved within the framework of one-dimensional (1D) models. However, notable ex-

ceptions are the works in Refs. [8–12], in which the electronic motion is described by including the full dimensionality of the problem, while the nuclear motion is being described in 1D.

Another difficulty with strong ir fields is that they induce distortions related to Stark shifts of molecular surfaces [13]. In order to circumvent these difficulties, LCEI in the high frequency, ultraviolet (uv) regime has been investigated [14], and many studies have been devoted to the field of molecular ionization and dissociation using xuv ultrashort laser pulses [15]. In the attosecond domain a pump-probe scheme involving xuv probe fields was proposed to map the time-dependent wave packets in D_2^+ [16], and ultrashort xuv pulses also offer new perspectives to explore attosecond LCEI [17]. Experiments based on high-order harmonic generation (HOHG) are now able to provide fs and sub-fs pulses in the xuv domain with high intensity [18–20], and HOHG has already been used to observe multiphoton ionization of atoms [21] and molecules [22]. Recently, the problem of dynamic imaging of an H_2^+ nuclear wave packet with brief laser pulses, was revisited [23]. The probe was an ultrashort (≤ 1 fs) xuv field linearly polarized along the internuclear axis. It was noticed that it is of crucial importance to take into account the underlying dependence of the ionization probability on the internuclear distance, when attempting to reconstruct the nuclear wave function from the kinetic energy distribution of the protons.

The aim of the present work is to pursue the study of the dynamics of an H_2^+ wave packet submitted to xuv fields, going beyond the sub-fs domain and considering different orientations of the molecule with respect to the polarization direction of the external field. We will focus on the limit of the fixed-nuclei approximation (FNA) [24,25] employing probe xuv pulse durations from the sub-fs to the fs domain. In particular, we investigate what effect the nuclear motion and the orientation of the molecule has on the kinetic energy distribution of the ejected protons. This is accomplished by numerical integration of the TDSE for the system beyond the Born-Oppenheimer (BO) approximation, exploring the behavior of the nuclei as the xuv field breaks the chemical

053415-1

bound. In the simulations, we simply assume that the initial H_2^+ wave packet has been created according to the Franck-Condon (FC) principle [26]. Such a wave packet may be produced from, e.g., electron impact ionization of H_2 [27]. However, we will also consider a case with a significantly colder initial vibrational distribution, since recent experimental studies on (tunneling) ionization of H_2 by infrared laser fields show that the actual distribution may deviate substantially from the conventional FC-like one [28]. A method to obtain the kinetic energy release (KER) spectra of the protons from the solutions of the TDSE within the FNA, which includes the vibrational distribution, is also developed, and the validity of this approximative approach is investigated in some detail.

II. THEORY

In the length gauge description of the light-matter interaction, the nonrelativistic dynamics of H_2^+ interacting with an external time-dependent and homogeneous electric field $\boldsymbol{E}(t)$ is governed by the TDSE

$$i\frac{\partial}{\partial t}\Psi(\boldsymbol{r},\boldsymbol{R},t) = [H(\boldsymbol{r},\boldsymbol{R}) + \boldsymbol{E}(t)\cdot\boldsymbol{r}]\Psi(\boldsymbol{r},\boldsymbol{R},t). \quad (1)$$

We use atomic units (a.u.) with $m_e = |e| = \hbar = a_0 = 1$, except where specified otherwise. The field-free (time-independent) Hamiltonian of the molecule is given by

$$H = -\frac{1}{2\mu}\nabla_R^2 - \frac{1}{2}\nabla_r^2 - \frac{1}{|\boldsymbol{r}+\boldsymbol{R}/2|} - \frac{1}{|\boldsymbol{r}-\boldsymbol{R}/2|} + \frac{1}{|\boldsymbol{R}|}, \quad (2)$$

where $\boldsymbol{r}$ is the electron coordinate measured from the center-of-mass of the nuclei, $\boldsymbol{R}$ is the internuclear vector, and μ is the reduced mass of the two nuclei. Introducing spherical coordinates, $\boldsymbol{r} = (r, \theta, \phi)$ and $\boldsymbol{R} = (R, \theta_R, \phi_R)$ for the electronic and internuclear coordinates, respectively, the reduced wave function $\Phi(\boldsymbol{r},\boldsymbol{R}) = rR\Psi(\boldsymbol{r},\boldsymbol{R})$, and imposing the additional constraint that the molecule is nonrotating and aligned along the positive z axis ($\theta_R = 0$), the resulting Hamiltonian becomes

$$H = -\frac{1}{2\mu}\frac{\partial^2}{\partial R^2} - \frac{1}{2}\frac{\partial^2}{\partial r^2} + \frac{L^2}{2r^2} + \frac{1}{R} + V_+ + V_-, \quad (3)$$

with

$$V_\pm = -\frac{1}{\sqrt{r^2 + \frac{1}{4}R^2 \pm rR\cos\theta}} \quad (4)$$

and $L(\theta, \phi)$ being the total angular momentum operator for the electronic motion.

The TDSE is solved numerically based on a recently developed split-step operator method in spherical coordinates [29,30]. Introducing $A = -\frac{1}{2}\frac{\partial^2}{\partial r^2}$, $B = -\frac{1}{2\mu}\frac{\partial^2}{\partial R^2}$, and $C = L^2/2r^2 + 1/R + V_+ + V_-$, the wave function at time $t + \Delta t$, with Δt small, can be evaluated approximately by the split-operator expression [31]

$$\Phi(\boldsymbol{r},\boldsymbol{R},t+\Delta t) \simeq e^{-i/2\Delta t A}e^{-i/2\Delta t B}e^{-i/2\Delta t C}e^{-i\boldsymbol{E}(t)\cdot\boldsymbol{r}\Delta t}$$
$$\times e^{-i/2\Delta t C}e^{-i/2\Delta t B}e^{-i/2\Delta t A}\Phi(\boldsymbol{r},\boldsymbol{R},t), \quad (5)$$

where the error made in each time step is of order Δt^2. An efficient and accurate numerical scheme is obtained by expanding the electronic wave function in spherical harmonics $Y_{lm}(\theta_j, \phi_k)$ defined on a finite set of points (θ_j, ϕ_k),

$$\Phi(r_i, \theta_j, \phi_k, R_n, t) = \sum_{lm} f_{lm}(r_i, R_n, t)Y_{lm}(\theta_j, \phi_k), \quad (6)$$

where r_i and R_n define the corresponding radial grid points. The grid representation in all coordinates makes the method very flexible, as it imposes no symmetry demands on the system, and accordingly, it is relatively straightforward to consider laser fields of arbitrary polarizations with respect to the internuclear axis. Correspondingly, the potentials $V_\pm$ are expanded in Legendre polynomials

$$V_\pm(\theta_j, \phi_k) = \sum_l \frac{r_<^l}{r_>^{l+1}}P_l(\cos\theta_j). \quad (7)$$

This expansion is especially well adapted to the numerical method we use to solve the TDSE, as it significantly reduces the number of spherical basis functions that has to be included in the expansion (6), in order to obtain (practically) converged results. In the present work, converged results were obtained by including spherical harmonics up to $l = 15$ in the expansion (6), with 1024 and 256 grid points in r and R, respectively, distributed evenly on the intervals $0 < r < 120$ a.u. and $0 < R < 10$ a.u. The latter values are chosen such that the wave packet does not reach the limit of the boxes during the pulse. An absorbing boundary is imposed at the edges in order to avoid (unphysical) reflections. We explicitly checked for convergence of the results by varying the density of grid points in the simulations, by conducting calculations in boxes of different sizes, and by varying the number of harmonics included in the expansions.

The initial nuclear wave packet $\chi(R, t=0)$ of H_2^+ is obtained by assuming that a direct vertical Franck-Condon transition from the vibrational ground state of H_2 has taken place at the time $t = 0$, in such a way that the ground vibrational state $X^1\Sigma_g^+(v=0)$ can be projected onto the complete set of BO vibrational states on the $H_2^+(1s\sigma_g)$ potential energy surface [23]. Then, in the case of free propagation, the time evolution of the FC wave packet for $t > 0$ is (trivially) given by

$$\chi(R, t) = \sum_v c_v \chi_v(R)e^{-i\epsilon_v t}, \quad (8)$$

where the coefficients c_v are determined by the initial conditions at $t = 0$. The stationary vibrational states χ_v and the corresponding energies ϵ_v of the molecular ion are obtained from the solutions of the eigenvalue problem

$$\left[-\frac{1}{2\mu}\frac{\partial^2}{\partial R^2} + E_{1s\sigma_g}(R)\right]\chi_v = \epsilon_v \chi_v \quad (9)$$

for the center-of-mass (c.m.) motion of the two protons on the $E_{1s\sigma_g}$ BO potential energy surface. Equation (9) is solved by expanding the functions $\chi_v(R)$ on a basis of B splines [23]. Moreover, the electronic ground-state wave function $\Phi_{1s\sigma_g}(r, R)$ and its corresponding R-dependent electronic energy $E_{1s\sigma_g}(R)$ are obtained at each fixed value of R by the technique of imaginary time propagation ($t \to \tau = -it$) of the

TDSE [25]. Then, the total wave function at a given delay time $\Delta T > 0$, after evolution in the absence of the laser field, is given by

$$\Phi(\mathbf{r}, R, \Delta T) = \Phi_{1s\sigma_g}(\mathbf{r}, R)\chi(R, \Delta T). \qquad (10)$$

The laser field that is assumed to be turned on at a given delay time $t = \Delta T$ is modeled by the classical electric field $\mathbf{E} = -\partial_t \mathbf{A}$, with the vector potential given as

$$\mathbf{A}(t) = \frac{E_0}{\omega}\sin^2\left[\frac{\pi}{T}(t - \Delta T)\right]\cos[\omega(t - \Delta T)]\mathbf{u}_p \qquad (11)$$

on the interval $\Delta T \leq t \leq \Delta T + T$, and zero elsewhere. Here, E_0 is the peak electric field amplitude, ω is the central frequency, T is the pulse duration, and the unit vector $\mathbf{u}_p$ defines the polarization of the linearly polarized field. In the following, we have studied both parallel and perpendicular polarization. In the first case, because of the axial symmetry of the problem, the m quantum number is a conserved quantity ($m=0$), which significantly reduces the complexity of the numerical calculations. However, for the perpendicular situation this symmetry is broken, with the result that different m states in the expansion (6) are populated throughout the pulse.

The final continuum wave function at the end of the laser pulse is obtained by eliminating the remaining population on bound and dissociative vibrational states. This is achieved by a projection on the (complete) set of (bound and dissociative) BO vibrational eigenstates that are supported by the box. These stationary states are obtained in a similar manner as described above. As a matter of fact, excitations to excited dissociative channels, such as, e.g., $2p\sigma_u$, $3p\sigma_u$, etc., are unlikely to occur for the xuv fields considered here.

In order to obtain the KER spectrum of the exploding nuclei, the total continuum wave function $\Phi_C(\mathbf{r}, R, t = \Delta T + T)$ at the end of the pulse is projected onto the exact Coulomb wave functions from the solutions of the eigenvalue problem [32] $H_N \chi_C = \epsilon \chi_C$, with $H_N(R) = -\frac{1}{2\mu}\frac{\partial^2}{\partial R^2} + \frac{1}{R}$ being the nuclear Hamiltonian, and ϵ the asymptotic kinetic energy of the exploding fragments. The solutions (normalized on the energy scale) are [33]

$$\chi_C(\epsilon, R) = N_\epsilon R \int_0^\infty dt(1 - \tanh^2 t)\cos(kR\tanh t - 2\mu t/k),$$

$$\qquad (12)$$

where $k = \sqrt{2\mu\epsilon}$ is the asymptotic momentum and

$$N_\epsilon = \frac{k}{\pi}\sqrt{1 - e^{-2\pi\mu/k}}. \qquad (13)$$

The c.m. nuclear KER spectrum thus becomes

$$\frac{dP(\epsilon)}{d\epsilon} = \int d^3r \left| \int_0^\infty dR\chi_C^*(\epsilon, R)\Phi_C(\mathbf{r}, R) \right|^2. \qquad (14)$$

In the full calculations, which is hereafter called the non-BO calculations, the TDSE in Eq. (1) is solved with the initial conditions given in Eq. (10).

We are now going to compare the results of the non-BO calculations with the results obtained within the fixed-nuclei approximation for various laser pulses. In the latter approach, which is hereafter referred to as the FNA, Eq. (1) is solved parametrically in such a way that the internuclear distance is held fixed during the calculation for each value of R. The ionization probability may then be obtained as a function of R. The final continuum electronic wave function, which now only depends parametrically on R, is then multiplied with the vibrational FC wave packet $\chi(R, \Delta T)$ given in Eq. (8). Finally, the KER spectrum is computed by formula (14), as in the full non-BO case. The approximation lies in the fact that we have assumed that the nuclear wave packet has not moved during the time of interaction with the pulse. The above procedure for reconstruction of the full wave packet from the FNA calculations is particularly useful as it allows one to compare the non-BO and FNA results directly. In the next section the applicability of the FNA to obtain the KER spectra for the ionization of an H_2^+ wave packet by xuv fields will be investigated in some detail.

III. RESULTS

First we briefly recall the context: at $t=0$ a short fs ir pulse ionizes H_2, leaving a Franck-Condon wave packet $H_2^+(1s\sigma_g, v)$. A second xuv field is applied at $t = \Delta T$. It ionizes H_2^+, and the KER spectrum is calculated. Figure 1 shows the KER spectrum $dP(\epsilon)/d\epsilon$ obtained at the delay time $\Delta T = 2.5$ fs for four different probe pulse durations lying in the interval 0.5 to 2.0 fs. The corresponding FNA results (dashed lines) are also shown for comparison. The number of field periods was always kept constant (equal to 20) in the calculations. This was accomplished by adjusting the pulse central frequency in each case, i.e., from $\omega = 6.08$ a.u. in Fig. 1(a) to $\omega = 1.52$ a.u. in Fig. 1(d). Likewise, the laser intensity was varied from case to case, so that the total ionization yield was always about 1%. The initial FC wave packet, that was centered about $R=2$ a.u. at $\Delta T = 2.5$ fs, is displayed in the inset in Fig. 5(b). At this point R the potential energy $E_{1s\sigma_g}(R)$ reaches its minimum value, and the (group) velocity of the wave packet is maximal. Hence, the validity of the fixed-nuclei approximation is expected to be most sensitive to the pulse duration for $\Delta T \simeq 2.5$ fs. And in fact, a gradual breakdown of the approximation as a function of the pulse duration is clearly seen in Figs. 1(a)–1(d).

It is worth noticing that, in contrast to [23], the present FNA calculations do not rely on Coulomb's law since the FNA kinetic energy spectrum is derived from Eq. (14). Therefore, the FNA spectra also include the contribution from the initial kinetic energy of the protons. This explains why the results of the full TDSE and the FNA calculations coincide in Fig. 1(a). As a matter of fact, due to the initial kinetic energy of the wave packet, a reconstruction of the probability density of the wave packet from the spectrum in Fig. 1(a) with aid of the Coulomb relation $\epsilon = 1/R$ would produce a wave function centered about a somewhat lower value of R than it should be. This is in agreement with Ref. [23]; nevertheless, we have checked that Coulomb's law is a reasonable approximation in the present context.
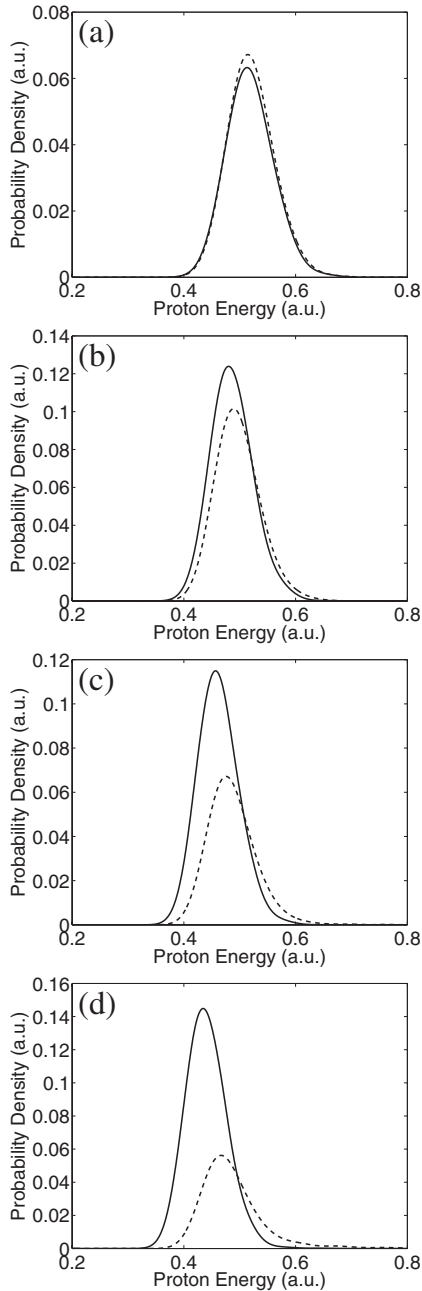
FIG. 1. Kinetic energy release (KER) spectra $dP(\epsilon)/d\epsilon$ of the H_2^+ wave packet taken at the delay time $\Delta T = 2.5$ fs versus total center-of-mass energy of the released nuclei, and for various probe pulse durations (a) 0.5 fs, (b) 1.0 fs, (c) 1.5 fs, and (d) 2.0 fs. Full and dashed lines indicate the result of the non-Born-Oppenheimer and fixed-nuclei approximation (FNA) calculations, respectively. The initial Franck-Condon (FC) wave packet that is peaked about $R = 2$ a.u. is shown in the inset in Fig. 5(b). The frequency of the linearly polarized xuv probe pulse is adjusted so that the number of field oscillations is kept constant and equal to 20 in each case, i.e., the central frequencies and peak electric field amplitudes are $\omega = 6.08$ a.u. and $E_0 = 2.0$ a.u. in (a), $\omega = 3.04$ a.u. and $E_0 = 0.54$ a.u. in (b), $\omega = 2.03$ a.u. and $E_0 = 0.24$ a.u. in (c), and $\omega = 1.52$ a.u. and $E_0 = 0.17$ a.u. in (d). The total ionization yields are 0.7% (0.7%), 1.2% (1.0%), 1.1% (0.7%), and 1.3% (0.6%), in (a)–(d) respectively, where the numbers in parenthesis give the corresponding FNA result.
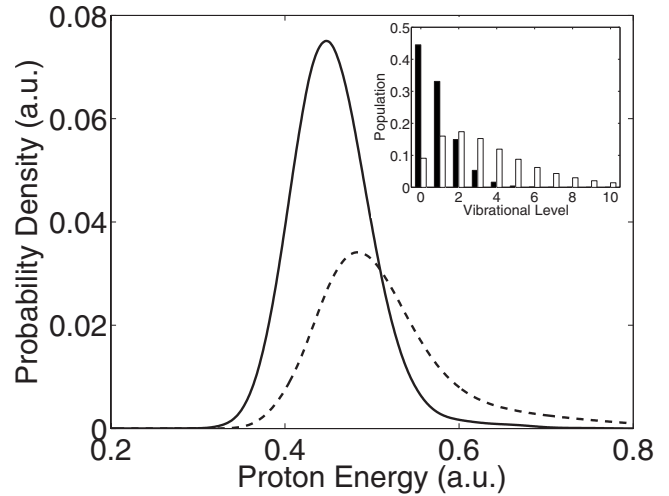

FIG. 2. The KER spectrum of the H_2^+ wave packet taken at the delay time $\Delta T = 2.5$ fs for a non-Franck-Condon wave packet [28]. The black bars in the inset indicate the non-FC distribution used in the calculation. For comparison, the FC distribution is indicated with white bars. The pulse parameters are the same as in Fig. 1(d). Full and dashed lines indicate the result of the non-BO and FNA calculations, respectively. The total ionization yields are 0.8% and 0.5% in the two cases.

We now turn to the case of longer pulse durations [Figs. 1(b)–1(d)]. The results of the non-BO and FNA calculations tend to differ in two important respects: First, the exact spectra (full lines) are shifted to lower proton energies as compared to the approximative ones, and the shift becomes more pronounced the longer the duration of the probe pulse. Second, the total ionization yields are higher in the full calculations, the results differing by a factor of more than two for the longest pulse. Since the wave packet is moving to larger internuclear distances during the duration of the pulse, a greater fraction of the wave packet will be ionized at larger values of R as compared to the case where the FC wave packet is assumed to stand still throughout the interaction time. Now, using Coulomb's law, this explains the shift of the non-BO spectra to lower proton energies for longer pulses. The difference in total ionization yields in the two approaches can be explained in a similar manner by referring to the insets in Figs. 3(a)–3(d). These insets show the ionization probability as a function of the internuclear distance obtained within the FNA, for each respective xuv laser pulse. All of them [except possibly the inset in Fig. 3(a)] show that the ionization probability increases as the wave function (that was initially centered about $R = 2$) moves to larger internuclear distances during the interaction. This explains the differences in ionization yields in Fig. 1, and the fact that the discrepancies are most pronounced for the longest pulses. All in all, the results in Fig. 1 suggest that caution should be made when employing the FNA in laser molecule interaction calculations, even for relatively short pulses.

Recently, it has been pointed out that the actual vibrational distribution in H_2^+ after ionization of H_2 molecules by an infrared laser field may deviate substantially from the conventional FC-like distribution [28,34]. This comes from the strong R dependence in the ionization rate. Therefore, in

order to accommodate such effects, we show in Fig. 2 the calculated kinetic energy distribution at the delay time $\Delta T = 2.5$ fs for a non-Franck-Condon-like distribution [28]. The laser parameters are given in Fig. 1(d). Although the non-FC distribution deviates significantly from the FC-like one (see inset in Fig. 2), we note the close resemblance of the results in Fig. 1(d) and Fig. 2. Hence, in the following paragraphs, we simply assume that the initial vibrational distribution is FC-like.

Figure 3 shows the same as Fig. 1, but in this case the probe pulse is applied at a much later delay time $\Delta T = 30$ fs. Now, the initial FC wave function, which is displayed in the inset in Fig. 5(c), has much more structure to it than in the previous example, and the kinetic energy distribution of the protons spans a much broader energy region. Although the overall shape of the spectra is the same in the non-BO and the FNA calculations, the results are shifted in energy relatively to each other. The shift becomes more pronounced the higher the kinetic energy of the released protons and the longer the duration of the pulse, as expected.

On the other hand, the (non-BO) spectra in Figs. 3(a)–3(d) are very different from each other, despite they all represent "an image" of the very same initial wave function. The discrepancy is especially prominent in the energy region near $\epsilon \simeq 0.5$ a.u. Using Coulomb's law once more, this corresponds to ionization near $R \simeq 2$ a.u. Now, the differences are readily understood by studying the R dependence of the ionization probability [insets in Figs. 3(a)–3(d)]. In the case in Fig. 3(a) the ionization probability goes through a (local) maximum in the immediate neighborhood of $R = 2$ a.u., whereas in the case in Fig. 3(d) the situation is almost reversed, i.e., the probability passes through a minimum value near $R = 2$ a.u. Hence, the variance in the results in Figs. 3(a)–3(d) can mainly be attributed to the difference in the R dependences in the ionization probabilities, i.e., to the central frequency of the applied xuv probe field. This particular example shows that one has to be very careful when attempting to apply Coulomb's law in order to reconstruct the initial FC wave packet from the KER spectrum.

It seems clear from the comparisons made in Figs. 1 and 3 that the fixed-nuclei approximation calculations provide, practically, exact results for pulses lasting less than 0.5 fs. Therefore, in the continuation the FNA is used to study the effect of the orientation of the molecule on the KER spectra, with emphasis on the difference between the parallel and perpendicular geometry. It is known from previous studies on the ionization of H_2^+ in xuv fields [35] that the ionization probability $P_{ion}(R)$ behaves differently depending on the orientation of the molecule with respect to the polarization direction of the field.

Figure 4 shows $P_{ion}(R)$ for two different orientations of the molecule, i.e., parallel and perpendicular with respect to the laser field, for an ultrashort laser pulse ($T = 0.25$ fs), with $\omega = 3.04$ a.u. and $E_0 = 1.21$ a.u. Such short pulses, or even shorter ones, are today experimentally available from high-harmonic generation [20]. As can be seen in the figure, the ionization is favored for shorter internuclear distances in both geometries. However, the molecule is much more easily ionized in the perpendicular geometry than in the case of perfect alignment. This difference will certainly play a sig-
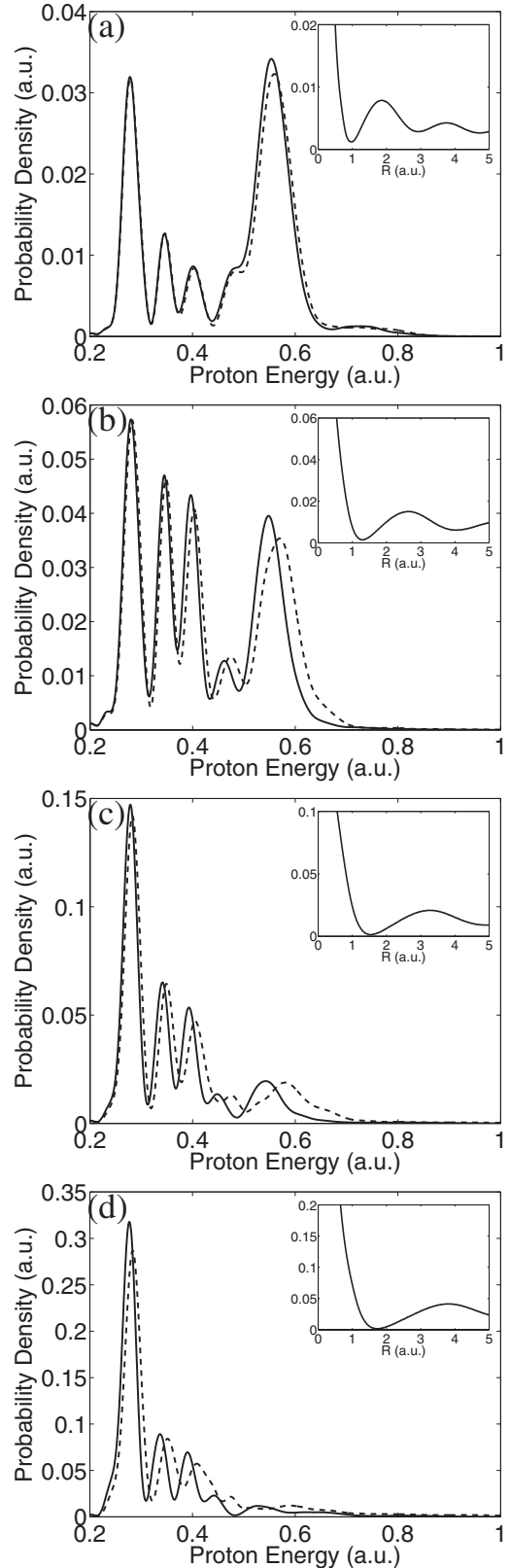

FIG. 3. As Fig. 1, but taken at a later delay time $\Delta T = 30$ fs. The insets show the ionization probability as a function of internuclear distance R obtained from the TDSE within the FNA. The initial FC wave packet is shown in the inset in Fig. 5(c). The total ionization yields are 0.5% (0.5%), 0.9% (0.9%), 1.2% (1.3%), and 1.9% (2.1%), in (a)–(d), respectively.
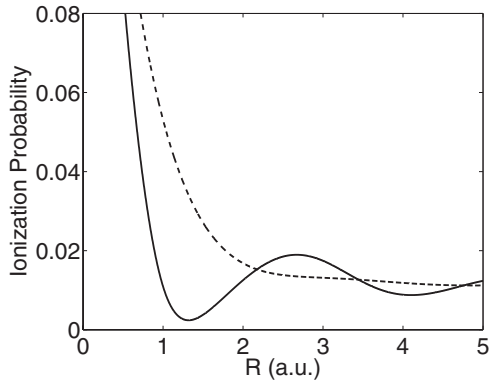
FIG. 4. Ionization probability of H_2^+ (obtained from the TDSE within the FNA) versus internuclear distance R, after interaction with a four-cycle (0.25 fs duration) laser pulse linearly polarized parallel (full line) and perpendicular (dashed line) to the internuclear axis. The central frequency $\omega = 3.04$ a.u. and peak electric field amplitude $E_0 = 1.21$ a.u.

nificant role in their respective KER spectra, especially at high proton energies. The oscillatory behavior of the ionization probability in the parallel geometry at larger internuclear distances, and the absence of these oscillations in the perpendicular geometry, can be understood within a simple two-center interference-diffraction model [36,35]. In this model one assumes that the electronic continuum wave function is a superposition of two outgoing spherical waves, one from each of the two scattering centers. If we make the additional assumption that the electron is ejected along the laser polarization direction, the total ionization probability becomes

$$P_{\text{ion}}(R) \propto [1 + \cos(k_e \mathbf{u}_p \cdot \mathbf{R})], \qquad (15)$$

where k_e is the momentum of the ejected electron. The interference factor (15) explains the different R dependence in Fig. 4.

Figure 5 shows the predicted KER spectra for parallel (full line) and perpendicular (dashed line) orientation of the molecule with respect to the linearly polarized field, and for three different delay times 0, 2.5, and 30 fs, respectively. The corresponding initial Franck-Condon wave packets are displayed in the insets. The field parameters were given in Fig. 4. As expected from the discussion around Fig. 4, the kinetic energy release spectra for parallel and perpendicular geometries, respectively, are indeed very different in the high energy region ($\epsilon > 0.5$ a.u.), the difference being less pronounced for $\epsilon < 0.5$ a.u. However, even at lower energies [see Fig. 5(c)], corresponding to ionization at $R > 2$ a.u., there are important discrepancies that can be explained by the interference factor in Eq. (15).

IV. CONCLUSIONS

In conclusion, we have carried out first principles non-Born-Oppenheimer (non-BO) calculations for the photoionization of an H_2^+ wave packet by a linearly polarized xuv field. In all cases, the electronic dynamics was solved in full dimensions, whereas for the nuclear motion, only the vibrational component was included, i.e., the rotation of the mol-
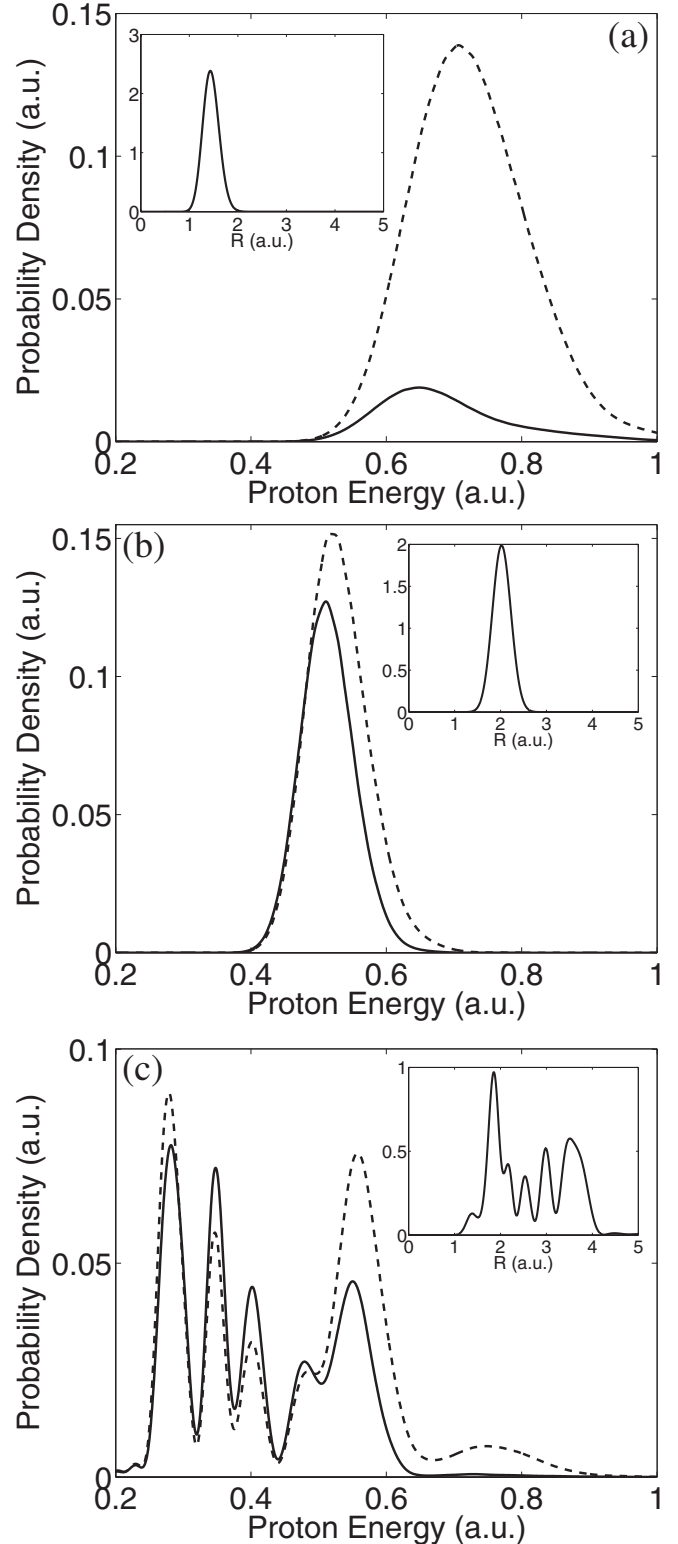

FIG. 5. KER spectra of the H_2^+ wave packet at different delay times, (a) $\Delta T = 0$ fs, (b) $\Delta T = 2.5$ fs, and (c) $\Delta T = 30$ fs, obtained with the xuv field linearly polarized parallel (full line) or perpendicular (dashed line) to the internuclear axis. The pulse parameters are given in Fig. 4. The insets show the initial FC wave packet at each delay time. The total ionization yields for parallel (perpendicular) polarization are 0.4% (2.9%), 1.2% (1.7%), and 1.2% (1.5%), in (a)–(c), respectively.

ecule, which is much slower than the vibrational motion, was neglected. The kinetic energy release (KER) spectra for the ejected nuclei were obtained for laser pulses of different durations and with varying central frequencies. Furthermore, we have calculated the corresponding spectra within the framework of the fixed-nuclei approximation (FNA) and compared the results with the predictions of the full non-BO model, in order to investigate the applicability of the FNA method in such kind of studies. We found that the FNA may not be valid at rather short pulse durations ($\sim$1.5 fs) in the region where the electronic potential is minimum ($R \simeq 2$ a.u.). The same conclusion may also be drawn for lower values of R, corresponding to high energetic protons. Finally, we have investigated the effect of the orientation of the molecule with respect to the polarization direction of the field, with emphasis on the case of parallel and perpendicular geometry. Due to the fact that the ionization probability in general depends on the internuclear distance from which the molecule is ionized, and the fact that this R dependence is different for different orientations of the molecule, the KER spectra also depend on the molecular orientation. In the perpendicular geometry, the KER signal is enhanced (compared to the parallel geometry) at short internuclear distances (corresponding to high kinetic energies), while the image of the wave packet is less deformed at larger values of R. Therefore, a measure of the KER spectrum in the perpendicular geometry should provide a more complete picture of the nuclear wave packet.

ACKNOWLEDGMENT

[1] A. Giusti-Suzor, F. H. Mies, L. F. DiMauro, E. Charron, and B. Yang, J. Phys. B **28**, 309 (1995).

[2] J. H. Posthumus, Rep. Prog. Phys. **67**, 623 (2004).

[3] P. Agostini and L. F. Di Mauro, Rep. Prog. Phys. **67**, 813 (2004).

[4] A. Scrinzi, M. Yu. Ivanov, R. Kienberger, and D. M. Villeneuve, J. Phys. B **39**, R1 (2006).

[5] A. Rudenko, Th. Ergler, B. Feuerstein, K. Zrost, C. D. Schröter, R. Moshammer, and J. Ullrich, J. Phys.: Conf. Ser. **88**, 012050 (2007).

[6] R. de Vivie-Riedle and U. Troppmann, Chem. Rev. (Washington, D.C.) **107**, 5082 (2007).

[7] D. S. Murphy, J. McKenne, C. R. Calvert, I. D. Williams, and J. F. McCann, New J. Phys. **9**, 260 (2007).

[8] S. Chelkowski, T. Zuo, O. Atabek, and A. D. Bandrauk, Phys. Rev. A **52**, 2977 (1995).

[9] V. Roudnev, B. D. Esry, and I. Ben-Itzhak, Phys. Rev. Lett. **93**, 163601 (2004).

[10] F. He, C. Ruiz, and A. Becker, Phys. Rev. Lett. **99**, 083002 (2007).

[11] S. Barmaki, H. Bachau, and M. Ghalim, Phys. Rev. A **69**, 043403 (2004).

[12] A. Palacios, H. Bachau, and F. Martín, J. Phys. B **38**, L99 (2005).

[13] A. D. Bandrauk and S. Chelkowski, Chem. Phys. Lett. **336**, 518 (2001).

[14] A. D. Bandrauk and S. Chelkowski, Phys. Rev. Lett. **87**, 273004 (2001).

[15] F. Martín, J. Phys.: Conf. Ser. **88**, 012001 (2007).

[16] X. M. Tong and C. D. Lin, Phys. Rev. A **73**, 042716 (2006).

[17] T. Okino, K. Yamanouchi, T. Shimizu, K. Furusawa, H. Hasegawa, Y. Nabekawa, and K. Midorikawa, Chem. Phys. Lett. **432**, 68 (2006).

[18] H. Mashiko, A. Suda, and K. Midorikawa, Opt. Lett. **29**, 1927 (2004).

[19] H. Mashiko, A. Suda, and K. Midorikawa, Appl. Opt. **45**, 573 (2006).

[20] M. Schultze, E. Goulielmakis, M. Uiberacker, M. Hofstetter, J. Kim, D. Kim, F. Krausz, and U. Kleineberg, New J. Phys. **9**, 243 (2007).

[21] H. Hasegawa, E. J. Takahashi, Y. Nabekawa, K. L. Ishikawa, and K. Midorikawa, Phys. Rev. A **71**, 023407 (2005).

[22] K. Hoshina, A. Hishikawa, K. Kato, T. Sako, K. Yamanouchi, E. J. Takahashi, Y. Nabekawa, and K. Midorikawa, J. Phys. B **39**, 813 (2006).

[23] S. Barmaki and H. Bachau, J. Phys. B **40**, 463 (2007).

[24] S. Barmaki, S. Laulan, H. Bachau, and M. Ghalim, J. Phys. B **36**, 817 (2003).

[25] S. Selstø, J. F. McCann, M. Førre, J. P. Hansen, and L. B. Madsen, Phys. Rev. A **73**, 033407 (2006).

[26] B. Feuerstein and U. Thumm, Phys. Rev. A **67**, 063408 (2003).

[27] F. von Busch and G. H. Dunn, Phys. Rev. A **5**, 1726 (1972).

[28] X. Urbain, B. Fabre, E. M. Staicu-Casagrande, N. de Ruette, V. M. Andrianarijaona, J. Jureta, J. H. Posthumus, A. Saenz, E. Baldit, and C. Cornaggia, Phys. Rev. Lett. **92**, 163004 (2004).

[29] J. P. Hansen, T. Sørevik, and L. B. Madsen, Phys. Rev. A **68**, 031401(R) (2003).

[30] T. Birkeland, M. Førre, J. P. Hansen, and S. Selstø, J. Phys. B **37**, 4205 (2004).

[31] M. R. Hermann and J. A. Fleck, Jr., Phys. Rev. A **38**, 6000 (1988).

[32] S. Chelkowski, A. D. Bandrauk, A. Staudte, and P. B. Corkum, Phys. Rev. A **76**, 013405 (2007).

[33] *Handbook of Mathematical Functions*, edited by M. Abramowitz and I. R. Stegun (Dover, New York, 1972), Eq. (14.3.3).

[34] T. K. Kjeldsen and L. B. Madsen, Phys. Rev. Lett. **95**, 073004 (2005).

[35] S. Selstø, M. Førre, J. P. Hansen, and L. B. Madsen, Phys. Rev. Lett. **95**, 093002 (2005).

[36] H. D. Cohen and U. Fano, Phys. Rev. **150**, 30 (1966).